Investigation of Structural, Electrical and Vibrational Properties of $Bi_{1.98}A_{0.02}Fe_4O_9$ (A= Ba, Ce) Multiferroic Ceramics

Poorva Sharma
Luzhou Vocational and Technical College
Ashwini Kumar (101101216@seu.edu.cn)
Southeast University

Research Article

Keywords: Ceramic, X-ray Diffraction, Raman Spectroscopy

Posted Date: December 21st, 2020

DOI: https://doi.org/10.21203/rs.3.rs-131866/v1

Abstract

In this paper, we report the synthesis, phase formation and basic characterization of polycrystalline $Bi_2Fe_4O_9$, $Bi_{1.98}Ba_{0.02}Fe_4O_9$, and $Bi_{1.98}Ce_{0.02}Fe_4O_9$ sample prepared through sol-gel route. Crystal structure of the as prepared samples have been characterized by X-ray diffraction and Raman scattering spectroscopy. All the obtained XRD peaks could be indexed to orthorhombic *Pbam* structure and revealed the formation of $Bi_2Fe_4O_9$. Raman spectrum identifies A_g, B_{2g} and B_{3g} active optical phonon modes. The size and morphology of the nanoparticles have been analyzed using scanning electron microscopy (SEM). Dielectric constant (e') decreases with increase in frequency and it is constant at higher frequencies region and it can be explained on the basis of ionic conduction phenomenon in the low frequency region. The value of e' for all $Bi_2Fe_4O_9$ based S1, S2, S3 and S4 samples are about 37, 75, 40 and 393, respectively at frequency 10 Hz. The observed properties signify that these materials are very useful in advanced technological and practical applications.

1. Introduction

Sol-gel processing, which gives a polycrystalline material, can control particle size of the crystallized phase and can eliminate any pores. We can also design the shape/form of precursor (bulk, thin-film, etc) [1]. In addition, metastable phases, which are hardly synthesized via solid-state route, often crystallize in ceramics prepared by Sol-gel route [2, 3]. Therefore, the processing has been studied intensively in order to produce the sophisticated functional materials. Crystal structure of $Bi_2Fe_4O_9$ is orthorhombic (*Pbam*) and belongs to family of mullite-type crystal structures [4, 5]. A unit cell of $Bi_2Fe_4O_9$ contains two formula units with evenly Fe ions distributed between octahedral (FeO_4) and tetrahedral (FeO_4) sites. In addition, Bi^{3+} ions are surrounded by eight oxygen ions. An unexpected multiferroic effect, which is observed as a coexistence of antiferromagnetism and ferroelectric polarization, was reported in $Bi_2Fe_4O_9$, attributed to frustrated spin system coupled with phonons [6]. The perovskite $BiFeO_3$ (BFO), which is both FE (T_{CE} =1103 K) and antiferromagnetic (AFM) (T_N=640 K), is one of the well-known multiferroics. However, it is difficult to obtain phase-pure BFO avoiding the formation of second phases during the conventional synthesis process. Various impurity phases have been reported to occur, such as $Bi_2Fe_4O_9$, $Bi_{46}Fe_2O_{72}$, and $Bi_{25}FeO_{40}$.[7, 8]. Among the impurity phases, $Bi_2Fe_4O_9$ is a well-known material, which has been extensively studied over the past several decades for various functional applications such as a semiconductor gas sensor and as a catalyst for ammonia oxidation [9–11].

Very recently, bulk $Bi_2Fe_4O_9$ were synthesized by solid state reaction and the multiferroic properties have been studied, displaying FE hysteresis loops at T = 250 K and AFM ordering T_N =260 K [12]. This shows that $Bi_2Fe_4O_9$ is one of the promising multiferroic materials. Whereas, impurity phases particularly Fe_2O_3 were existed in the samples, which could affect the magnetic and FE properties of polycrystalline $Bi_2Fe_4O_9$ ceramics. Studies of electric and dielectric properties are also equally important from both fundamental and application point of view. Dielectric and magnetic behavior of ferrites is greatly

influenced by an order of magnitude of conductivity and is mostly dependent on preparation method and sintering conditions [7].

In this paper, we have synthesized the pristine $Bi_2Fe_4O_9$ and Ce^{3+} and Ba^{2+} ion modified $Bi_2Fe_4O_9$ to improve its structural and physical properties. Individually, both of the Ce^{3+} and Ba^{2+} ions were doped at Bi-site in $Bi_2Fe_4O_9$. In order to obtain the proper phase of ceramic we examine the phase formation and physical properties, the glassy precursor was subjected to different heat-treatment at different temperatures for different time duration. Despite the evident importance of $Bi_2Fe_4O_9$ as a functional material, very few reports have appeared. Here, we report the phase formation, physical properties and vibrational properties of polycrystalline $Bi_2Fe_4O_9$ ceramic synthesized by a sol-gel route.

2. Experimental Details

2.1 Synthesis

$Bi_2Fe_4O_9$, $Bi_{1.98}Ba_{0.02}Fe_4O_9$, $Bi_{1.98}Ce_{0.02}Fe_4O_9$ ceramics have been successfully synthesized by sol-gel route. High purity nitrates were carefully weighed and stoichiometrically mixed. It utilizes multifunctional organic acids capable of chelating metal ions into stable complexes. Suitable metal salts are introduced into the Ethylene Glycol, Citric acid, which is added in large excess to form metal citrates.

$Bi_2Fe_4O_9$

Precursors of bismuth nitrate and iron nitrate are taken in specific ratio (molar ratio). Appropriate deionized water was added to dissolve and solution was then stirred on magnetic stirrer. While stirring citric acid was introduced as a complexant and pH value (6–7) is maintained by adding ammonia [12]. Temperature is supplied to form gel up to 100 °C and after that xero-gel was completely burnt to form ashes. Then calcination is done at 650 °C for 2 h. For the same powder we did second calcination again at 850 °C for 2 h and observe the changes. In another heating treatment the calcination was done at 800 °C and then after grinding again calcined at 850 °C. Obtained powder was then ground in agate mortar and pestle. Finally, the pellets were sintered at temperature 850 °C for 8 hrs, respectively.

Ba and Ce doped $Bi_2Fe_4O_9$

Nitrates of Bi, Fe, Ba and Ce are taken in specific molar ratio. Appropriate deionized water was added to dissolve and solution was then stirred on magnetic stirrer. While stirring citric acid was introduced as a complexant and pH value (6–7) is maintained by adding ammonia. Temperature was supplied to form gel up to 100 °C and after that xero-gel was completely burnt to form ashes. First calcination was done at 650 °C and second calcination was done at 850 °C with intermediate grinding. Finally, the pellets were sintered at temperature 850 °C for 8 hrs.

2.2 Experimental techniques

X–ray diffraction (XRD) pattern were taken using CuKα1 radiation (λ = 1.5406 Å) of a Bruker D8 Advance X-ray diffractometer. The sample morphology was investigated with a scanning electron microscope (JEOL, JSM-5600). Raman measurements on as synthesized sample was carried out on Jobin-Yovn Horiba LABRAM (System HR800) spectrometer with a 632.8 nm excitation source equipped with a Peltier cooled CCD detector. Dielectric measurements were made as a function of frequency in the range of 100 Hz – 1 MHz on Novocontrol alpha-ANB impedance analyzer at room temperature.

3. Results And Discussion

3.1 Crystal structure analysis

Room temperature XRD pattern of $Bi_2Fe_4O_9$ and Ba and Ce-doped $Bi_2Fe_4O_9$ samples as prepared by Sol-gel route is shown in Fig. 1(a-d). As we mentioned before the $Bi_2Fe_4O_9$ samples were calcined at different temperatures are further designated as $(Bi_2Fe_4O_9)650–850$ for $Bi_2Fe_4O_9$ calined at 650°C and 850°C and $(Bi_2Fe_4O_9)800–850$ for $Bi_2Fe_4O_9$ sample calcined at 800°C and 850°C. Finally these both samples have been sintered at 850 °C (8 h). For the samples $(Bi_2Fe_4O_9)650–850$ and $(Bi_2Fe_4O_9)800–850$ the diffraction peaks are well indexed with the orthorhombic structure of $Bi_2Fe_4O_9$ (space group: *Pbam*), matche well with JCPDS card No. 74-1098 [13] with no trace of other impurity phases within the limit of instrument sensitivity. These result confirms that phase-pure $Bi_2Fe_4O_9$ can be synthesized by sol-gel route. From Fig. 1(a, b), we can observe the broading of the peaks in $(Bi_2Fe_4O_9)650–850$ sample due to low calcination temperature. Whereas, due to high calcination temperature, proper crystalline phase has been observerd in $(Bi_2Fe_4O_9)800–850$ sample. Due to calcination temperature variation double peaks transforms into a single peak from sample $(Bi_2Fe_4O_9)650–850$ to $(Bi_2Fe_4O_9)800–850$. Furthermore, the refined lattice parameters of sample $(Bi_2Fe_4O_9)650–850$ are a = 7.94 Å, b = 8.40 Å, and c = 5.92 Å; and a = 7.95 Å, b = 8.45 Å, c = 5.94 Å for $(Bi_2Fe_4O_9)800–850$, revealing the slight expansion in both the *ab* plane and the c axis with doping contents increasing. In addition, with the increase of calcination temperature, there is a limited intensity increasing and narrowing of the diffraction peaks, indicative of better crystallization and the increase of crystalline sizes. Using the Debye Scherrer formula, the average crystalline size can be estimated to be about 52 nm, 80 nm for $(Bi_2Fe_4O_9)650–850$ and $(Bi_2Fe_4O_9)800–850$.

XRD for alkaline earth metal Ba^{+2} ion and rare earth Ce^{+3} ion doped $Bi_2Fe_4O_9$ ceramics are shown in Fig. 1(c, d). For the doped samples the diffraction peaks are well indexed with the orthorhombic structure of $Bi_2Fe_4O_9$ (space group: *Pbam*), matches well with (JCPDS: 25–0090). As witnessed from the Fig. 1(c,d) in the doped $Bi_2Fe_4O_9$ samples, there is a shift in lower theta value due to ionic radius mismatch of dopent (ionic radius of Ba = 1.35, Ce = 1.01) with Bi^{+3} (0.96) ion. The ionic radius of Ba and Ce ions are greater then Bi ion that is why we are getting a shifting at lower theta value as comparison to parent $Bi_2Fe_4O_9$ ceramic. The lattice parameters were obtained using indexing such as *a* = 7.101 Å, b = 8.50 Å, and c = 5.94 Å for $Bi_{1.98}Ba_{0.02}Fe_4O_9$, and *a* = 7.99 Å, b = 8.48 Å, and c = 5.93 Å for $Bi_{1.98}Ce_{0.02}Fe_4O_9$

sample. The crystalline size for Ce^{+3} and Ba^{+2} ions doped ceramics are found to be 62 and 65 nm, respectively

3.2 Microstructure analysis

The scanning electron microscope (SEM) was used to study the surface morphological and microstructural characteristics of pristine and doped $Bi_2Fe_4O_9$ compound. Figure 2(a-d) shows typical SEM images of pristine and doped $Bi_2Fe_4O_9$ samples. Compared with the pristine $Bi_2Fe_4O_9$ sample, the grains of the doped $Bi_2Fe_4O_9$ sample are randomly oriented and have the smaller grain size. The average grain size is estimated to be about 65 nm. As we can see in the SEM images, the particles of all these four samples are agglomerated and little porous in nature. Therefore, we can say that the particle size increses with increasing the calcination temperature as we can see in SEM image of $(Bi_2Fe_4O_9)800–850$ sample. The typical SEM images reveals that microstructures are dense comprising of non-uniform grains with varying particles size indicating polycrystalline nature of as prepared samples. The SEM image also showed some poros among the loosely connected grains in the sample.

3.3 Raman scattring analysis

Raman spectrum of $Bi_2Fe_4O_9$ at room temperature is depicted in Fig. 3(a-d). The Raman active modes of the structure can be summarized using the irreducible representation $12A_g + 12B1_g + 9B2_g + 9\ B3_g$, which is employed to describe Raman modes of orthorhombic (*Pbam* space group) [13]. In the measured Raman spectra of $(Bi_2Fe_4O_9)650–850$, the A_g modes are existed at 83, 95, 115, 122, 139, 222, 289 and 607 cm^{-1}. The agreement between experimental and predicted values is relatively good for the all frequency modes, dominated by Bi vibrations. The Raman peak centered at 472 cm^{-1} is might be attributed to magnetic ordering effect on phonon line width consistent with earlier observation of bands at ~ 260 and 472 cm^{-1} due to magnon scattering. Similarly, for $(Bi_2Fe_4O_9)800–850$ the obtained Raman A_g modes are at 91, 206, 282, 326, 365, 430, 554, and 640 cm^{-1}. We can analyze there are number of modes decreasing due to increasing in calcination temperature. The A_g modes for $Bi_{1.98}Ba_{0.02}Fe_4O_9$ are following (53, 93, 119, 183, 209, 313, 446 and 558 cm^{-1}). Similarly, for $Bi_{1.98}Ce_{0.02}Fe_4O_9$ the A_g modes are at 53, 68, 118, 183, 206, 308, 442, 560 cm^{-1}. It would be more practical to study the magnetic excitations in $Bi_2Fe_4O_9$ under the assumption that they involve two-magnon processes, like in the well-known cases of ferrites [14] or cuprates [12, 15]. At higher frequency (> 250 cm^{-1}), it is unlikely the magnetic-order-induced bands correspond to one-magnon excitations but in rare-earth orthoferrites ($RFeO_3$; R = Dy, Ho, Er, Sm etc.) have frequencies below 25 cm^{-1} for comparison the zone-center magnons [16].

3.4 Dielectric response

The real part of permittivity (ε') as a function of frequency of $Bi_2Fe_4O_9$ based ceramics at room temperature is shown in Fig. 4(a-d).The value of ε' for all $Bi_2Fe_4O_9$ based samples are about 37, 75, 40 and 393 for $(Bi_2Fe_4O_9)650–850$, $(Bi_2Fe_4O_9)800–850$, $(Bi_{1.98}Ba_{0.02}Fe_4O_9)$, and $(Bi_{1.98}Ce_{0.02}Fe_4O_9)$

samples, respectively at frequency 10 Hz. At higher frequency (~ 1 MHz), the values of ε' are 11.68, 12.90, 5.06 and 5.36 respectively for ($Bi_2Fe_4O_9$)650–850, ($Bi_2Fe_4O_9$)800–850, ($Bi_{1.98}Ba_{0.02}Fe_4O_9$), and ($Bi_{1.98}Ce_{0.02}Fe_4O_9$) samples, respectively. The above is comparable with the previous measurements pure $Bi_2Fe_4O_9$. Dielectric constant (ε') decreases with increase in frequency and it is constant at higher frequencies region. From Fig. 4 we have found that the value of dielectric constant in the whole frequency range (100 Hz– 1 MHz) is nearly constant in the prepared ceramics. This result appears to be consistent with our previous empirical analysis using the Maxwell–Wagner model with thermal activation across multiple band gaps in isolated impurities [17]. The dielectric loss (tanδ) as a function of frequency of $Bi_2Fe_4O_9$ based ceramics at room temperature is shown in Fig. 5. We have observed that the value of dielectric loss is low for ($Bi_2Fe_4O_9$)650–850 among the entire prepared sample, dielectric relaxation are possible in all prepared sample.

4. Conclusions

In conclusion, the polycrystalline samples of ($Bi_2Fe_4O_9$)650–850, ($Bi_2Fe_4O_9$)800–850, ($Bi_{1.98}Ba_{0.02}Fe_4O_9$), and ($Bi_{1.98}Ce_{0.02}Fe_4O_9$) samples were successfully prepared by sol-gel route. By the indexing of X-ray diffraction data confirms the formation of $Bi_2Fe_4O_9$ phase having orthorhombic structure of $Bi_2Fe_4O_9$ (space group: *Pbam*). There is no evidence for structural change in the as prepared samples. Raman spectra reveal the presence of magnon peak is only in ($Bi_2Fe_4O_9$)650–850 sample. Thus, we can say at lower calcination temperature there is improvement in particle size. The value of ε' for all $Bi_2Fe_4O_9$ based ($Bi_2Fe_4O_9$)650–850, ($Bi_2Fe_4O_9$)800–850, ($Bi_{1.98}Ba_{0.02}Fe_4O_9$), and ($Bi_{1.98}Ce_{0.02}Fe_4O_9$) samples are about 37, 75, 40 and 393, respectively at frequency 10 Hz. At higher frequency (~ 1 MHz) the values of ε' are 11.68, 12.90, 5.06 and 5.36 for ($Bi_2Fe_4O_9$)650–850, ($Bi_2Fe_4O_9$)800–850, ($Bi_{1.98}Ba_{0.02}Fe_4O_9$), and ($Bi_{1.98}Ce_{0.02}Fe_4O_9$) samples, respectively. Dielectric constant (*i.e.* ε') decreases with increase in frequency and it is constant at higher frequencies region. The value of dielectric loss is low for ($Bi_2Fe_4O_9$)650–850 among the entire prepared sample, dielectric relaxation is possible in all as prepared samples. The decrease in dielectric constant with increased frequency could be explained on the basis of ionic conduction phenomenon in the low frequency region.These properties make this material very useful in technological and practical applications.

Declarations

Acknowledgement:

Authors acknowledge the Luzhou Vocational and Technical College for providing us start-up research grants.

References

1. Sakamoto A, Yamamoto S (2010) Int J Appl Glass Sci 1:237–247
2. Furukawa T, White WB (1980) J Mater Sci 15:1648–1662
3. Shioya K, Komatsu T, Kim HG, Sato R, Matusita K (1995) J Non-Cryst Solids 189:16
4. Johnson JA, Schweizer S, Lubinsky AR (2007) J Am Ceram Soc 90:693–698
5. Takahashi Y, Nakamura K, Osada M, Fujiwara T (2012) Sci Rep 2:714
6. Honma T, Ito N, Togashi T, Sato A, Komatsu T (2013) J Power Sources 227:31–34
7. Kumar MM, Srinivas A, Suryanarayana SV (2000) J Appl Phys 87:855
8. Selbach SM, Einarsrud MA, Grande T (2009) Chem Mater 21:169
9. Koizumi H, Niizeki N, Ikeda T, Jpn (1964) J Appl Phys 3:495
10. Zakharchenko NI (2000) Russ J Appl Chem 73:2047
11. Poghossian AS, Abovian HV, Avakian PB, Mkrtchian SH, Haroutunian VM (1991) Sens Actuators B 4:545
12. Litvinchuk AP, Börjesson L, Thomsen C, Chu CW (1999) Phys Status Solidi B 215:507
13. Park YA, Song KM, Hur N (2008) J Korean Physical Society 53:3356
14. Massey MJ, Baier U, Merlin R, Weber WH (1990) Phys RevB 41:7822
15. Holmlund J, Knee CS, Andreasson J, Granath M, Litvinchuk AP, Börjesson L (2009) Phys Rev B 79:085109
16. White RM, Nemanich RJ, Herring C Phys. Rev. B (1982) 25 1822
17. Shukla A, Choudhary RNP (2012) J Mater Sci 47:5074

Figures

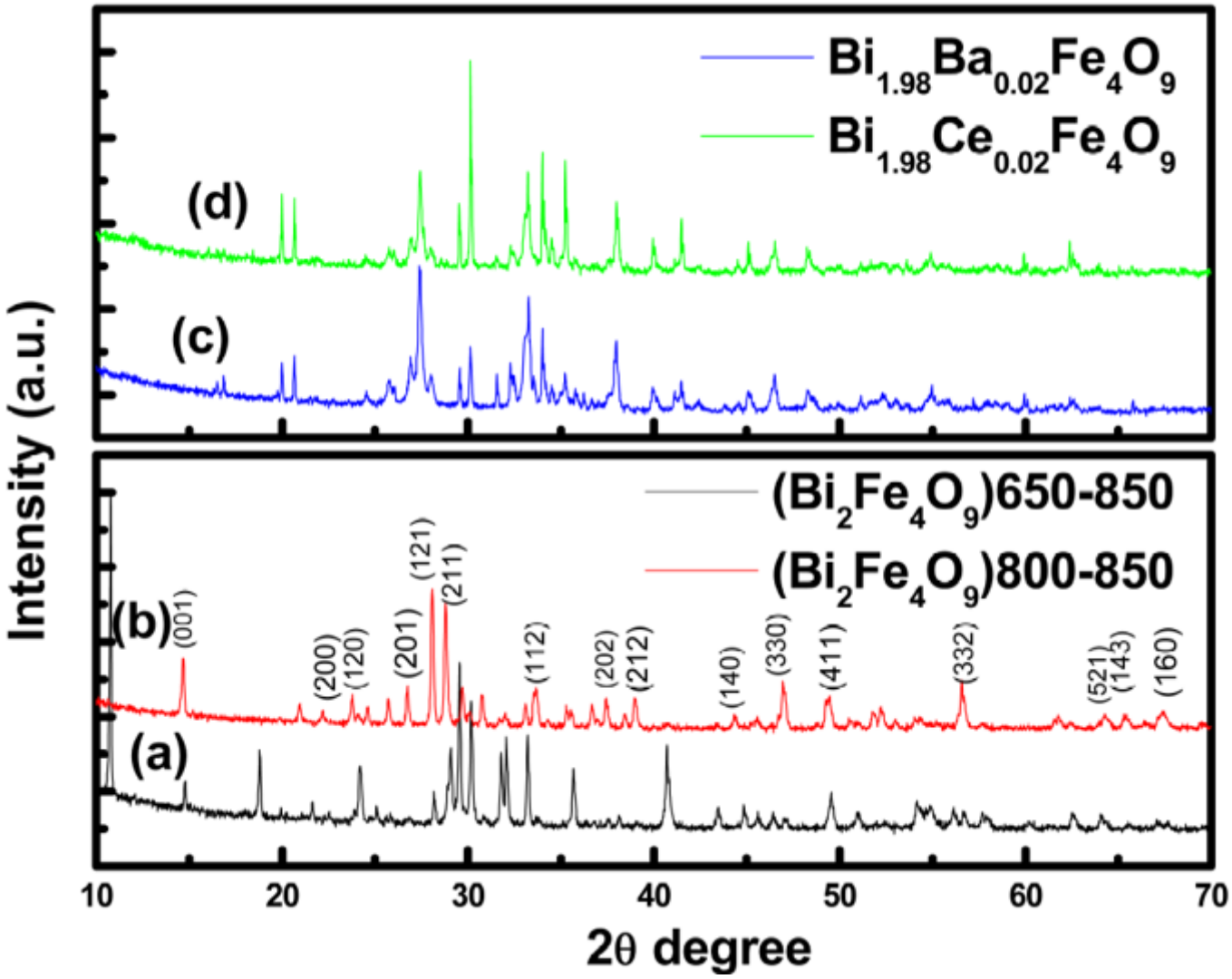

Figure 1

XRD pattern for undoped and doped Bi2Fe4O9 samples.

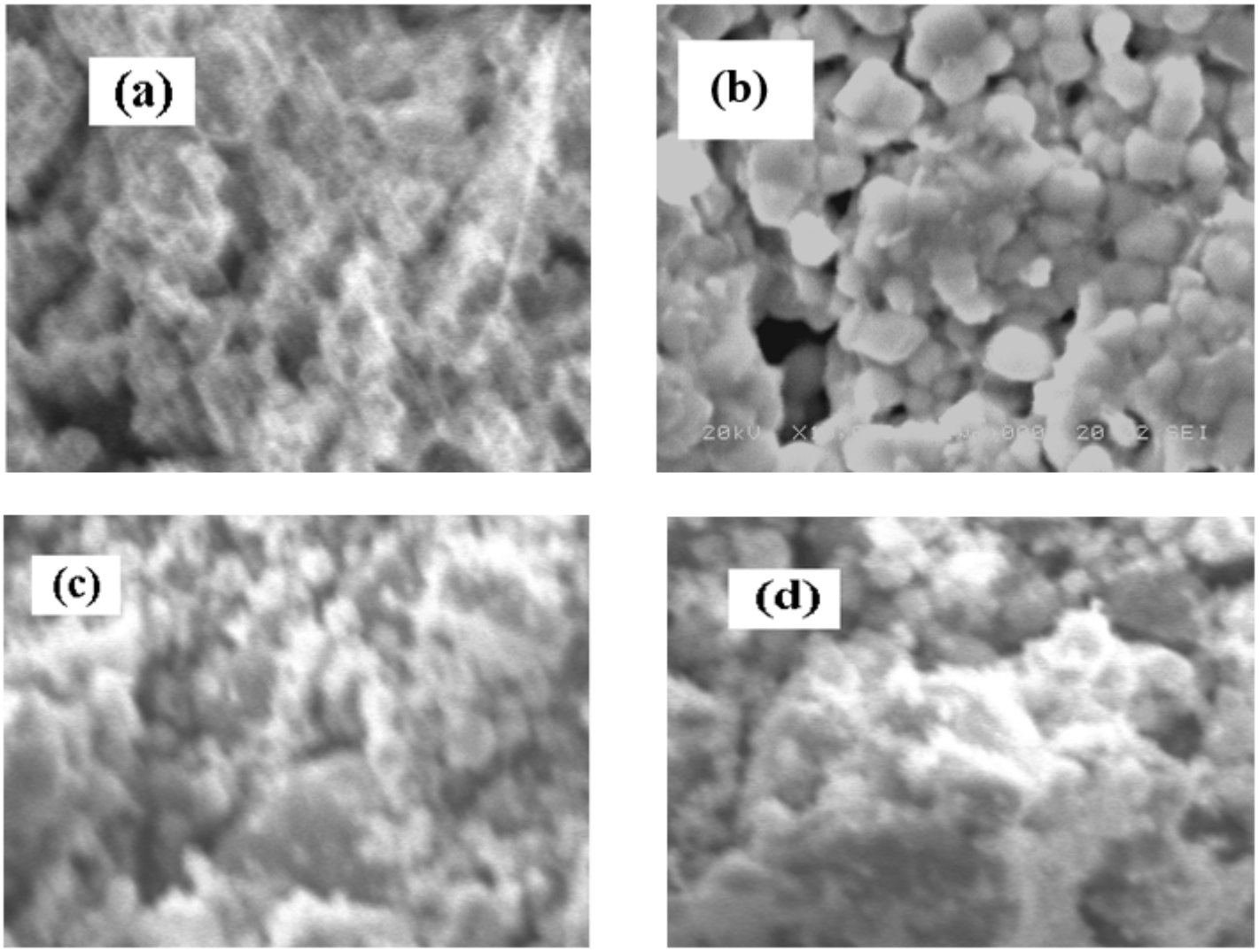

Figure 2

Scanning electron microscope images of the as-prepared Bi2Fe4O9 based samples.

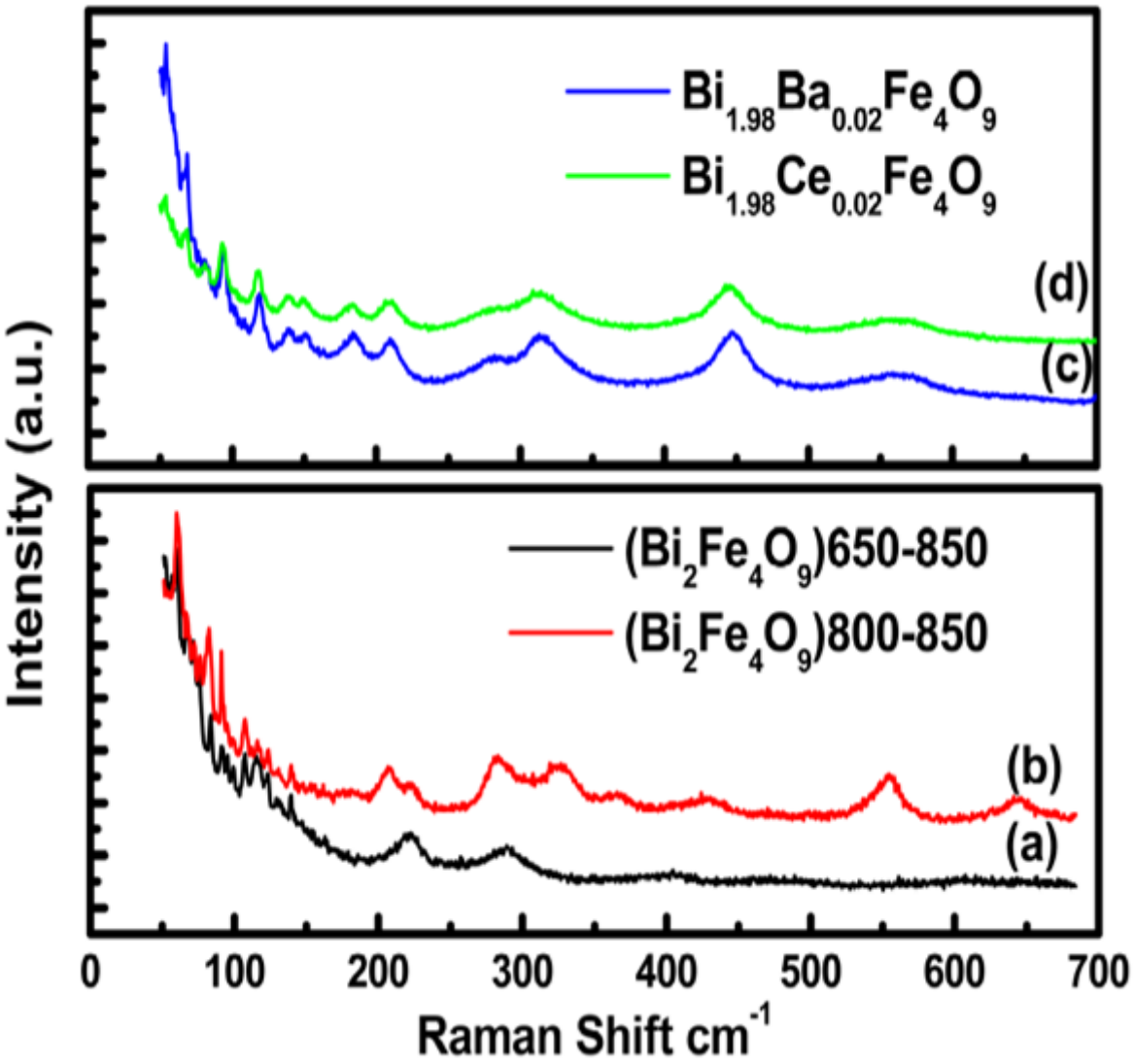

Figure 3

Raman spectra for undoped and doped Bi2Fe4O9 samples.

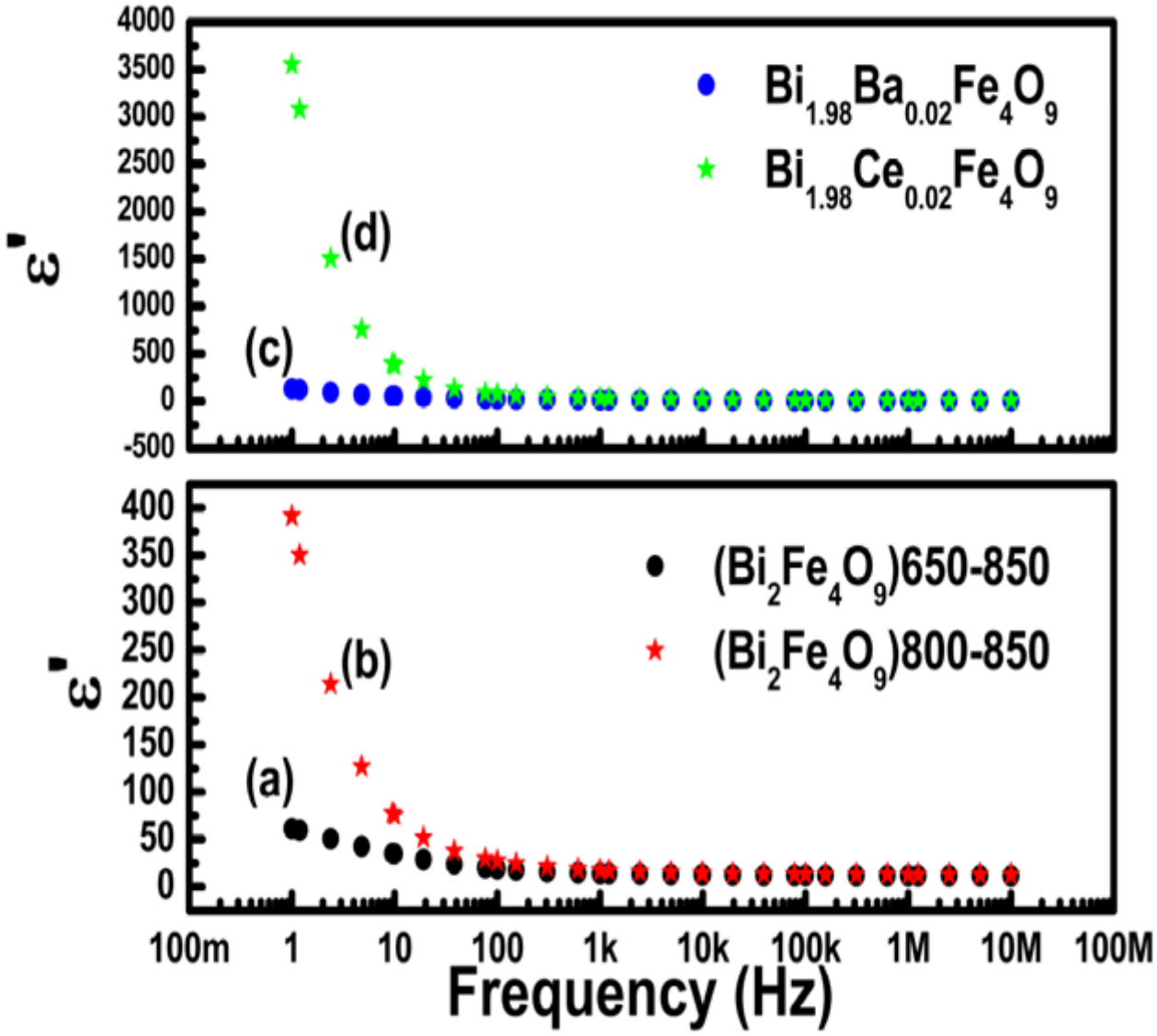

Figure 4

Dielectric constant behavior for undoped and doped Bi2Fe4O9 samples.

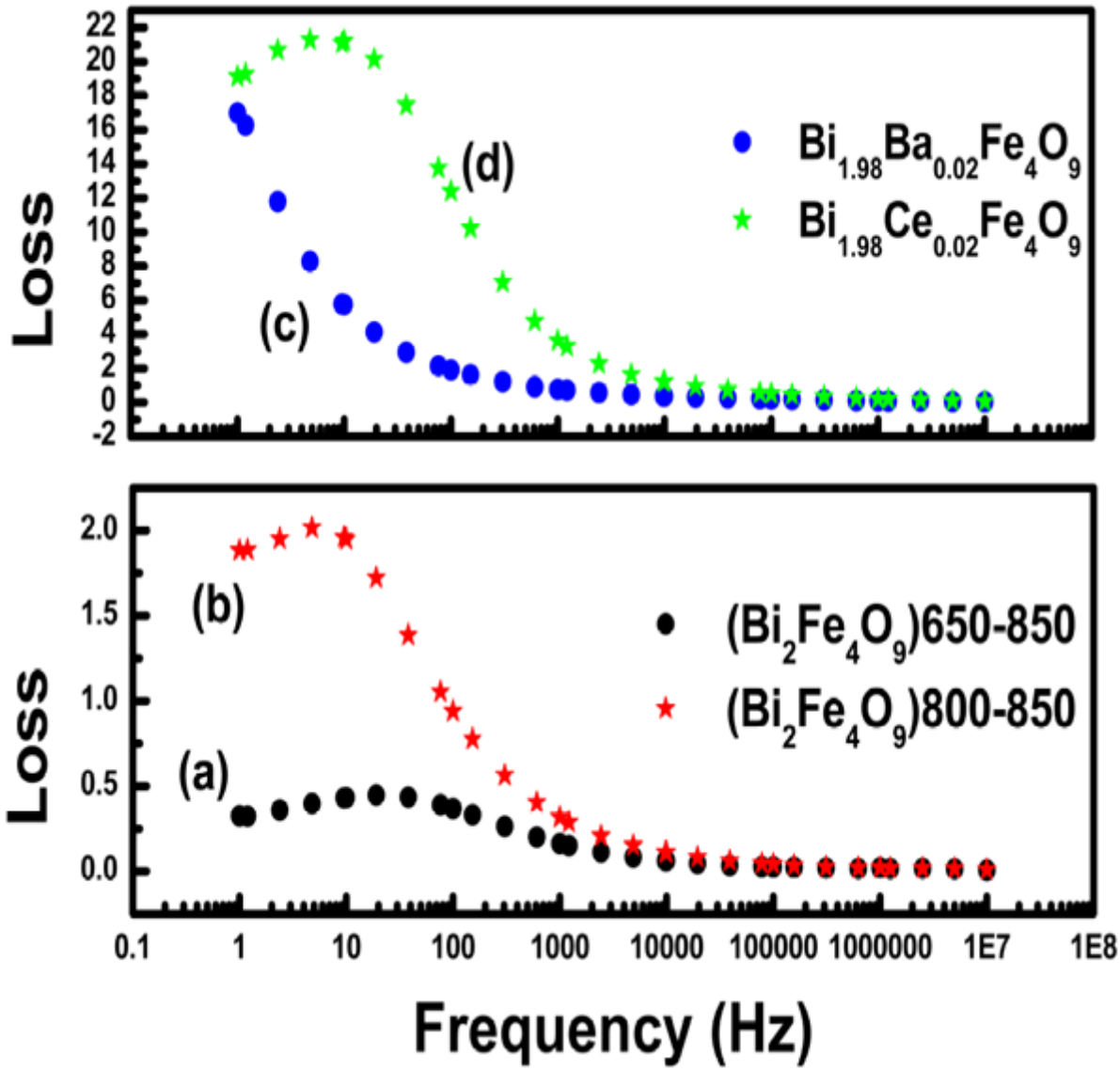

Figure 5

Dielectric loss behavior for undoped and doped Bi2Fe4O9 samples.